frontiers | Frontiers in Chemistry

PERSPECTIVE
published: 28 June 2022
doi: 10.3389/fchem.2022.919552

High Lithium Storage Performance of Co Ion-Doped $Li_4Ti_5O_{12}$ Induced by Fast Charge Transport

M. Wang[1,2], Y. Chen[1], C. X. Yang[1], Y. H. Zeng[1], P. F. Fang[1], W. Wang[1] and X. L. Wang[1,2]*

[1]School of Materials Science and Engineering, Liaoning Technical University, Fuxin, China, [2]Key Laboratory of Mineral High Value Conversion and Energy Storage Materials of Liaoning Province, Fuxin, China

In this study, Co_3O_4-doped $Li_4Ti_5O_{12}$ (LTO) composite was designed and synthesized by the hydrothermal reduction method and metal doping modification method. The microstructure and electrochemical performance of the Co_3O_4-doped $Li_4Ti_5O_{12}$ composite were characterized by XRD, SEM, TEM, electrochemical impedance spectroscopy, and galvanostatic tests. The results showed that $Li_4Ti_5O_{12}$ particles attached to lamellar Co_3O_4 constituted a heterostructure and Co ion doped into $Li_4Ti_5O_{12}$ lattice. This Co ion-doped microstructure improved the charge transportability of $Li_4Ti_5O_{12}$ and inhibited the gas evolution behavior of $Li_4Ti_5O_{12}$, which enhanced the lithium storage performance. After 20 cycles, the discharge specific capacity reached stability, and the capacity retention maintained 99% after 1,000 cycles at 0.1 A/g (compared to the capacity at the 20th cycle). It had an excellent rate performance and long cycle stability, in which the capacity reached 174.6 mA h/g, 2.2 times higher than that of $Li_4Ti_5O_{12}$ at 5 A/g.

Keywords: metallic ion doping, Li4Ti5O12, charge transport, lithium storage performance, the microstructure

OPEN ACCESS

Edited by:
Meng Zheng,
Qingdao Haiwan Science and Technology Industry Research Institute Co., Ltd., China

Reviewed by:
Xiao Lyu,
Shenyang Ligong University, China
Yong Yan,
Beijing University of Technology, China

****Correspondence:***
M. Wang
wangming@lntu.edu.cn

Specialty section:
This article was submitted to Electrochemistry, a section of the journal Frontiers in Chemistry

Received: *13 April 2022*
Accepted: *26 April 2022*
Published: *28 June 2022*

Citation:
Wang M, Chen Y, Yang CX, Zeng YH, Fang PF, Wang W and Wang XL (2022) High Lithium Storage Performance of Co Ion-Doped $Li_4Ti_5O_{12}$ Induced by Fast Charge Transport. Front. Chem. 10:919552. doi: 10.3389/fchem.2022.919552

INTRODUCTION

Lithium-ion batteries have the advantages of high energy density, high charge transport rate, long cycle life, high security, and no memory effect. Therefore, it has been widely used in the field of consumer electronics and electric vehicles (Chen et al., 2013; Liu et al., 2013; Yang et al., 2015a; Yang et al., 2015b; Liu et al., 2015; Li Z et al., 2016; Li H. Z et al., 2016; Li S et al., 2016; Qu et al., 2018; Lu et al., 2019). $Li_4Ti_5O_{12}$ (LTO) was widely studied as anode material for lithium-ion batteries due to its good electrochemical performance (Zhang et al., 2013; Sun et al., 2014; Yan, 2014; You et al., 2018; Wang, 2020; Wang, 2021). However, the low theoretical specific capacity, the low charge transport rate, and the poor electrical conductivity led to serious polarization during rapid charge and discharge, which greatly limited its wide application (Shen et al., 2012; Kim et al., 2013; Zettsu et al., 2014; Tan and Xue, 2018). In recent years, many researchers have carried out several modification studies of pure LTO, including carbon coating, ion doping, and nanocrystallization. (Tang et al., 2009; Cheng et al., 2010; Shi et al., 2011; Li et al., 2013; Ma et al., 2013; Wang et al., 2013; Cheng et al., 2014; Li et al., 2014; Liu et al., 2014; Zhang et al., 2021). In this study, layered Co_3O_4 and spherical LTO heterostructures with large specific surface area and short ion diffusion length were prepared by the ion doping method. The composite has excellent electrochemical performance using the microstructure characterization and electrochemical performance test.

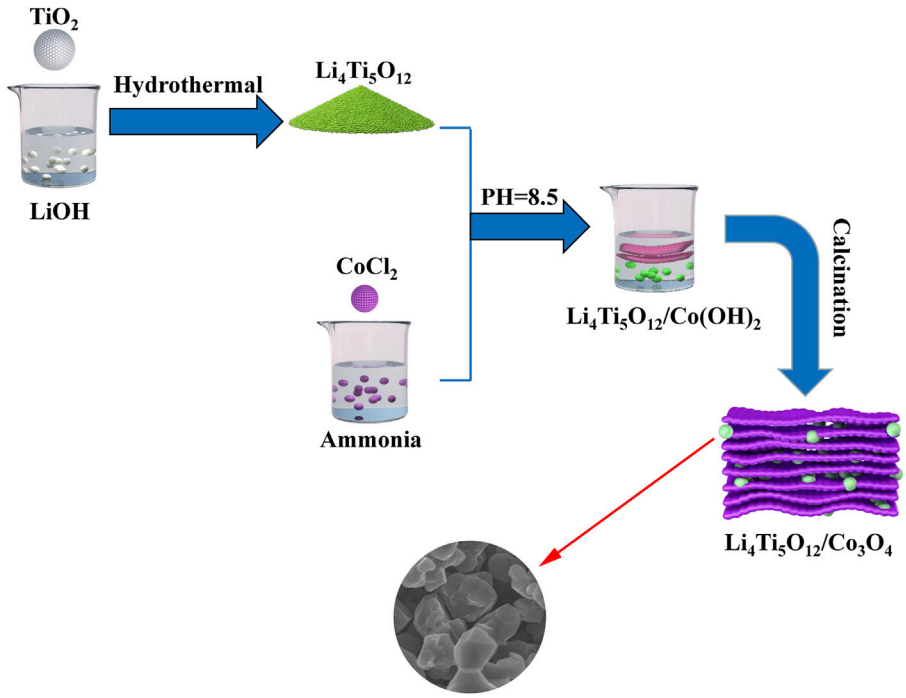

FIGURE 1 | Schematic diagrams of the synthesis of the $Li_4Ti_5O_{12}/Co_3O_4$ composite.

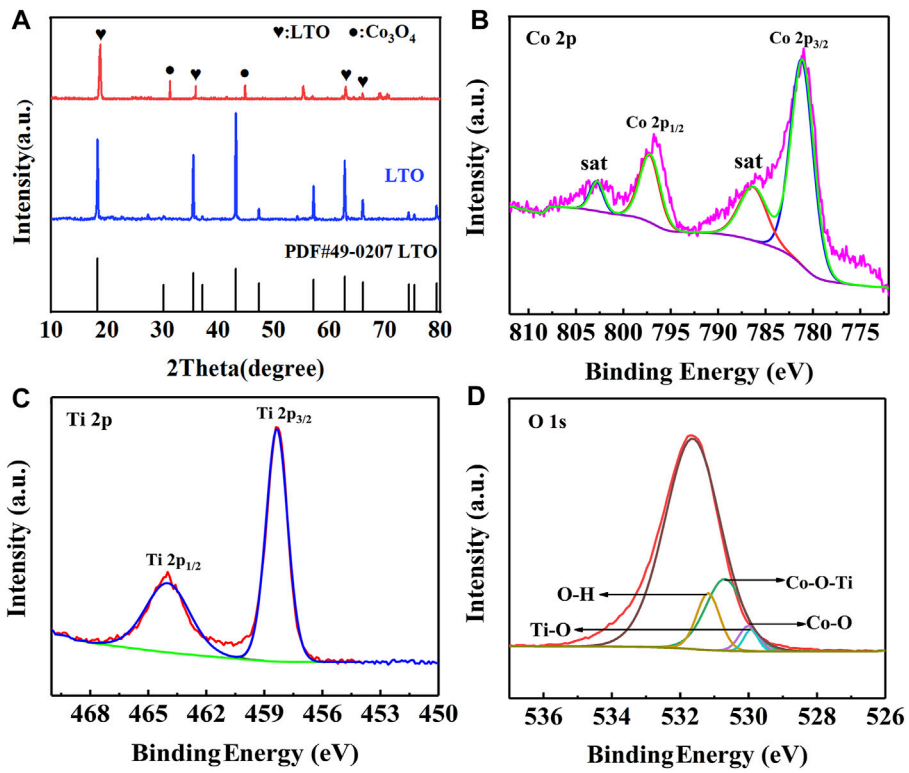

FIGURE 2 | (A) XRD patterns of $Li_4Ti_5O_{12}$ and $Li_4Ti_5O_{12}/Co_3O_4$ composite. **(B–D)** XPS patterns of $Li_4Ti_5O_{12}/Co_3O_4$ composite. **(B)** Co 2p; **(C)** Ti 2p; **(D)** O 1s.

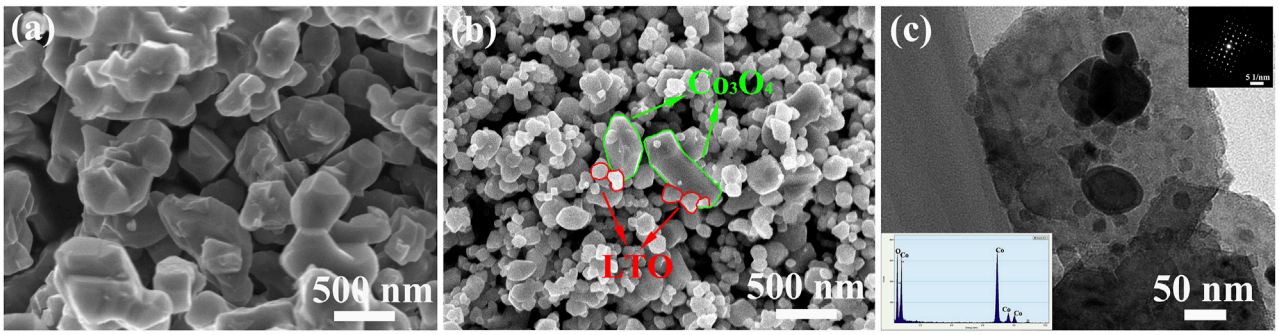

FIGURE 3 | (A) SEM image of $Li_4Ti_5O_{12}$ particles; **(B)** SEM image of $Li_4Ti_5O_{12}/Co_3O_4$ composites; **(C)** TEM morphology of $Li_4Ti_5O_{12}/Co_3O_4$ composites (inset: EDS of the Co_3O_4 sheet and SAED pattern of $Li_4Ti_5O_{12}$ particle).

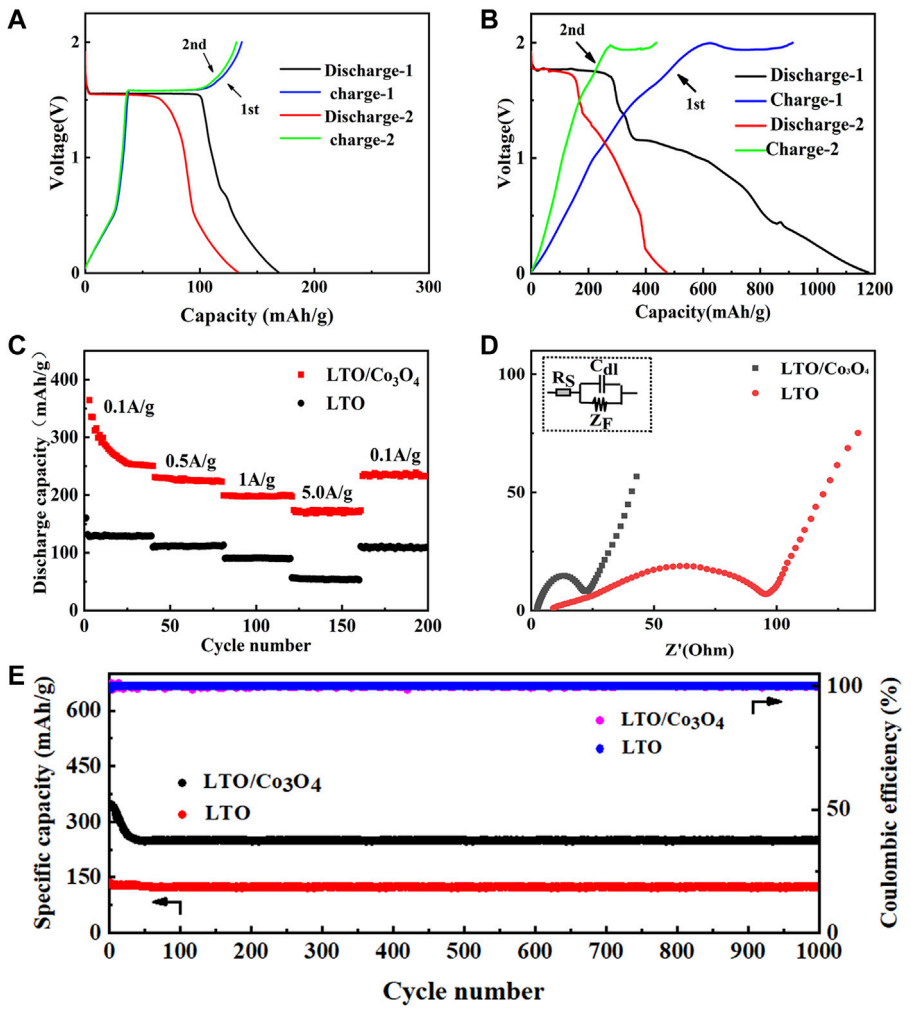

FIGURE 4 | (A) The first and second charge/discharge curves of $Li_4Ti_5O_{12}$. **(B)** The first and second charge/discharge curves of $Li_4Ti_5O_{12}/Co_3O_4$. **(C)** The rate performance comparison of $Li_4Ti_5O_{12}$ and $Li_4Ti_5O_{12}/Co_3O_4$. **(D)** The EIS (AC impedance) diagram of $Li_4Ti_5O_{12}$ and $Li_4Ti_5O_{12}/Co_3O_4$. **(E)** Cycle performance curves comparison of $Li_4Ti_5O_{12}$ and $Li_4Ti_5O_{12}/Co_3O_4$ at 0.1A/g.

EXPERIMENTAL

Firstly, 1.5 mg of $CoCl_2$ was dissolved in 30 ml dilute ammonia solution (0.3 mol/L). The pH value of the above solution was adjusted to 8.5 by concentrated ammonia solution and stood for 12 h. The formed precipitate (α-$Co(OH)_2$) was filtered and dried. Then, a certain mass of α-$Co(OH)_2$, LiOH, and TiO_2 was mixed and placed in a 100 ml Teflon-lined stainless steel autoclave and heated at 90°C for 12 h. After the temperature was cooled to room temperature, the solution was filtered and dried. The precursors were heated at 800°C for 4 h in a tube furnace. The obtained product was LTO/Co_3O_4 powder. Finally, CR2025-type coin cells were assembled in a high-purity Ar-filled ZKX glovebox. The schematic diagram of the synthesis of the LTO/Co_3O_4 composite is shown in **Figure 1**.

The phase composition of the specimen was characterized by XRD (SHIMADZU XRD-6100). The microstructure and morphology of the specimen were analyzed by SEM (JSM-7500F) and FEI TEM (Tecnai G2T20). The charge and discharge performance, rate performance, cycle performance, and Coulombic efficiency, among others, were tested on the battery performance test system (NEWARE). Electrochemical impedance spectroscopy (EIS) was tested on the CHI660E electrochemical workstation.

RESULTS AND DISCUSSION

The XRD pattern of LTO and LTO/Co_3O_4 composites prepared by the hydrothermal method is shown in **Figure 2**. It was found that the diffraction peak of the LTO/Co_3O_4 composite at 18.3°, 35.6°, 62.8°, and 66.1° corresponded to the crystal planes of (111), (311), (440), and (531), respectively. The characteristic diffraction peak of Co_3O_4 at 31.3° and 44.8° corresponded to the crystal planes of (220) and (440), respectively. In addition, it was observed that the diffraction peak of the LTO/Co_3O_4 composite shifted significantly to the right. For the (111) crystal plane of LTO, when Co ions were doped into the LTO lattice, the diffraction peak of the composite shifted to the right at approximately 0.5°; the reason for the radius of the Co atom (1.26 Å) was less than that of the Ti atom (1.45 Å), indicating that LTO and Co_3O_4 have a good combination.

The surface chemical composition and interfacial bonding state of the LTO/Co_3O_4 composite were analyzed by XPS, as shown in **Figure 2**. The high-resolution spectra of Co 2p, Ti 2p, and O 1s are shown in **Figures 2B–D**, respectively. It can be seen from **Figure 2B** that the two signal peaks located at 795.7 and 779.8 eV corresponded to the Co $2p_{3/2}$ and Co $2p_{1/2}$ of Co 2p, respectively, and each diffraction peak was accompanied by a satellite peak (Yang et al., 2022). The two characteristic peaks of Ti 2p at 464.3 and 458.6 eV were the spin-orbital peaks of Ti $2p_{1/2}$ and Ti $2p_{3/2}$, respectively (see **Figure 2C**), which was consistent with Zhou's results (Zhou et al., 2006). In addition, **Figure 2D** shows the Ti-O, Co-O, O-H, and Co-O-Ti bonds, four diffraction peaks, corresponding to 529.9, 530.0, 532.1, and 530.7 eV, respectively. The formation of the Co-O-Ti bond was successfully induced by hydrothermal synthesis of the LTO/Co_3O_4 composite, which was consistent with the reports in the literature (Xu et al., 2020). There is a synergistic effect between the surface of LTO and Co_3O_4, which can effectively improve the electrochemical performance of the composite. At the same time, the unsaturated O atoms in the composite combined with H atoms in water to form an O-H bond. It can also be seen from **Figure 2D** that the peak intensity of the Ti-O bond was significantly lower than that of the Co-O-Ti bond; the reason for the formation of the Co-O-Ti bond weakened the Ti-O bond, indicating that Co ions were successfully doped into LTO lattice.

Figure 3 shows the SEM morphology and the TEM morphology of LTO and LTO/Co_3O_4 composite. **Figure 3A** shows that the diameters of pure LTO nanoparticles were approximately 200 nm. It can be seen from **Figure 3B** that LTO spherical nanoparticles were uniformly attached to the surface and interlayer of Co_3O_4, in which the particle size of LTO was approximately 50 ± 20 nm and the lamellar diameter of Co_3O_4 was approximately 150 ± 50 nm. The addition of Co_3O_4 effectively inhibited the growth of LTO nanoparticles. The grain refinement would improve the specific surface area of the composite (Li et al., 2018). **Figure 3C** shows that the LTO nanoparticles were uniformly dispersed on the layered surface of Co_3O_4, indicating that LTO and Co_3O_4 combined well. In addition, EDS analysis showed that the composite contained Co and O elements, indicating the existence of Co_3O_4 in the composite (see the inset of **Figure 3C**).

The first and second charge/discharge curves of LTO and LTO/Co_3O_4 composite at 0.1 A/g are shown in **Figures 4A,B**, respectively. It can be seen that the first discharge specific capacity of LTO and LTO/Co_3O_4 composite was 175 and 1,178.0 mA h/g, and the first Coulomb efficiency was 76.3% and 77.6%, respectively. The addition of Co_3O_4 improved the ion diffusion rate of the composite, increasing the first discharge specific capacity of the composite. In addition, the second discharge specific capacity of LTO and LTO/Co_3O_4 composite was 133.2 and 473 mA h/g, respectively. The first and second discharge specific capacity of LTO and LTO/Co_3O_4 composite was quite different. The reason was that the anode material would form SEI film at the electrode/electrolyte interface after the first cycle, which consumed part of Li^+, causing irreversible capacity loss. Compared with LTO (1.55 V vs. Li/Li^+ (Wang et al., 2016)), the discharge voltage platform of the LTO/Co_3O_4 composite was 1.75 V (vs. Li/Li^+). The higher discharge voltage platform was beneficial in inhibiting the growth of lithium dendrites and forming a stable SEI film, which improves the cycle performance of the composite. **Figure 4C** shows the rate performance of LTO and LTO/Co_3O_4 composite for 200 cycles at different current densities. The discharge specific capacity of LTO/Co_3O_4 composite was higher than that of LTO at different current densities, indicating better rate performance. The discharge specific capacity of LTO at 20, 60, 100, and 140 cycles corresponded to 128.8, 110.9, 91.1, and 53.6 mA h/g, respectively. After 160 cycles, the discharge specific capacity was stable at 111.1 mA h/g, and the capacity retention rate was 86.3% (compared to the capacity at the 20th cycle). The discharge specific capacity of LTO/Co_3O_4 at 20, 60, 100, and

140 cycles corresponded to 274.5, 226.2, 201.1, and 174.6 mA h/g, respectively. After 160 cycles, the discharge specific capacity was stable at 230.6 mA h/g, and the capacity retention rate was 84% (compared to the capacity at the 20th cycle). The EIS (AC impedance) test results of LTO and LTO/Co_3O_4 composite are shown in **Figure 4D**. The curve in **Figure 4D** was fitted by an analog circuit, where R_S is ohmic resistance, C_{dl} is the double capacitance between electrode and electrolyte, and Z_F is the series connection between R_{CT} (charge transfer resistance) and Z_W (Warburg resistance). The results showed that the internal resistance of LTO and LTO/Co_3O_4 composite was 9.0 and 2.5 Ω, and the charge transfer resistance was 95.4 and 19.5 Ω, respectively. Compared with pure LTO, the LTO/Co_3O_4 composite has lower resistance because the incorporation of Co_3O_4 provided more charge transfer channels, improving the charge transport rate of the LTO/Co_3O_4 composite. The long cycle performance of the LTO/Co_3O_4 composite at 0.1 A/g for 1,000 cycles is shown in **Figure 4E**. **Figure 4E** shows that the discharge specific capacity of the composite decreased significantly in the first 20 cycles due to the continuous formation of SEI, leading to the continuous decomposition of Li^+. With the increase in the cycle number, the SEI film gradually tended to be stable and the discharge specific capacity loss was smaller. After 1,000 cycles, the discharge specific capacity of the LTO and LTO/Co_3O_4 composite was maintained at 124.3 and 248.4 mA h/g, and the capacity retention rate reached 96.5% and 99% (compared to the capacity at the 20th cycle), respectively. The LTO/Co_3O_4 composite combined with the advantage of Co_3O_4 (the high discharge specific capacity) and LTO (the good cycle stability).

The geometric structure model of LTO, Co_3O_4, and LTO/Co_3O_4 was optimized based on the density functional theory. As shown in **Supplementary Figure S1A**, 0 eV was defined as the Fermi level. The bandgap between the conduction band and the valence band was 0.8 eV, indicating that the composite exhibited semi-metallic properties. In addition, the energy value of the LTO/Co_3O_4 composite was higher than that of LTO and Co_3O_4 at the Fermi level (see **Supplementary Figure S1B**). The synergistic effect between LTO and Co_3O_4 significantly increased the probability of electrons appearing in the LTO/Co_3O_4 composite at the Fermi level, which was more conducive to electron transfer, improving the charge transfer rate of the LTO/Co_3O_4 composite.

CONCLUSION

The Co ion-doped LTO composite was prepared using the hydrothermal method. The combination of LTO and Co_3O_4 by the Co-O-Ti bond not only maintained the structural stability of the composite but also improved the electron/ion diffusion rate of the composite. Compared with LTO, LTO/Co_3O_4 has a higher first discharge specific capacity, good rate performance, and better cycle stability. The first specific capacity was 1,178 mA h/g at 0.1 A/g. After 1,000 cycles, the discharge specific capacity was 248.4 mA h/g and the capacity retention rate was 99% (compared to the capacity at the 20th cycle). At the same time, the LTO/Co_3O_4 composite also has a higher discharge specific capacity at high current density (the discharge specific capacity was 174.6 mA h/g at 5 A/g), which was 2.2 times that of pure LTO.

DATA AVAILABILITY STATEMENT

The original contributions presented in the study are included in the article/**Supplementary Material**. Further inquiries can be directed to the corresponding author.

AUTHOR CONTRIBUTIONS

MW: resources, writing—review and editing, supervision, project administration, funding acquisition. YC and CXY: designing and completing experiments, writing—original draft. YHZ, PFF, and WW: investigation, writing—review and editing. XLW: funding acquisition.

FUNDING

This work was financially supported by the National Natural Science Foundation of China (51974152), General Project of Science Research Foundation of Liaoning Province (LJKZ0363), Central Government Guiding Local Project of Science and Technology Development Foundation (2022JH6/100100047), and Discipline Innovation Team Project of Liaoning Technical University (LNTU20TD-09 and LNTU20TD-16).

SUPPLEMENTARY MATERIAL

The Supplementary Material for this article can be found online at: https://www.frontiersin.org/articles/10.3389/fchem.2022.919552/full#supplementary-material

Supplementary Figure S1 | (A) The energy band diagram of $Li_4Ti_5O_{12}/Co_3O_4$ and **(B)** the density of states of $Li_4Ti_5O_{12}$, Co_3O_4, and $Li_4Ti_5O_{12}/Co_3O_4$.

REFERENCES

Chen, Z., Belharouak, I., Sun, Y.-K., and Amine, K. (2013). Titanium-Based Anode Materials for Safe Lithium-Ion Batteries. *Adv. Funct. Mat.* 23 (8), 959–969. doi:10.1002/adfm.201200698

Cheng, J., Che, R., Liang, C., Liu, J., Wang, M., and Xu, J. (2014). Hierarchical Hollow $Li_4Ti_5O_{12}$ Urchin-like Microspheres with Ultra-high Specific Surface Area for High Rate Lithium Ion Batteries. *Nano Res.* 7 (7), 1043–1053. doi:10.1007/s12274-014-0467-2

Cheng, L., Yan, J., Zhu, G.-N., Luo, J.-Y., Wang, C.-X., and Xia, Y.-Y. (2010). General Synthesis of Carbon-Coated Nanostructure $Li_4Ti_5O_{12}$as a High Rate

Electrode Material for Li-Ion Intercalation. *J. Mat. Chem.* 20 (3), 595–602. doi:10.1039/b914604k

Kim, J.-G., Shi, D., Park, M.-S., Jeong, G., Heo, Y.-U., Seo, M., et al. (2013). Controlled Ag-Driven Superior Rate-Capability of $Li_4Ti_5O_{12}$ Anodes for Lithium Rechargeable Batteries. *Nano Res.* 6 (5), 365–372. doi:10.1007/s12274-013-0313-y

Li, H., Shen, L., Wang, J., Ding, B., Nie, P., Xu, G., et al. (2014). Design of a Nitrogen-Doped, Carbon-Coated $Li_4Ti_5O_{12}$ Nanocomposite with a Core-Shell Structure and its Application for High-Rate Lithium-Ion Batteries. *ChemPlusChem* 79 (1), 128–133. doi:10.1002/cplu.201300316

Li, H. Z., Yang, L. Y., Liu, J., Li, S. T., Fang, L. B., Lu, Y. K., et al. (2016). Improved Electrochemical Performance of Yolk-Shell Structured SnO 2 @void@C Porous Nanowires as Anode for Lithium and Sodium Batteries. *J. Power Sources* 324, 780–787. doi:10.1016/j.jpowsour.2016.06.011

Li, N., Zhou, G., Li, F., Wen, L., and Cheng, H.-M. (2013). A Self-Standing and Flexible Electrode of $Li_4Ti_5O_{12}$ Nanosheets with a N-Doped Carbon Coating for High Rate Lithium Ion Batteries. *Adv. Funct. Mat.* 23 (43), 5429–5435. doi:10.1002/adfm.201300495

Li, S., Liu, G., Liu, J., Lu, Y., Yang, Q., Yang, L.-Y., et al. (2016). Carbon Fiber cloth@VO_2(B): Excellent Binder-free Flexible Electrodes with Ultrahigh Mass-Loading. *J. Mat. Chem. A* 4 (17), 6426–6432. doi:10.1039/c6ta00728g

Li, W., Wang, F., Ma, M., Zhou, J., Liu, Y., and Chen, Y. (2018). Preparation of SiO_2 Nanowire Arrays as Anode Material with Enhanced Lithium Storage Performance. *RSC Adv.* 8 (59), 33652–33658. doi:10.1039/c8ra06381h

Li, Z., Ding, F., Zhao, Y., Wang, Y., Li, J., Yang, K., et al. (2016). Synthesis and Electrochemical Performance of $Li_4Ti_5O_{12}$ Submicrospheres Coated with TiN as Anode Materials for Lithium-Ion Battery. *Ceram. Int.* 42, 15464–15470. doi:10.1016/j.ceramint.2016.06.198

Liu, J., Lu, P.-J., Liang, S., Liu, J., Wang, W., Lei, M., et al. (2015). Ultrathin Li_3VO_4 Nanoribbon/graphene Sandwich-like Nanostructures with Ultrahigh Lithium Ion Storage Properties. *Nano energy* 12, 709–724. doi:10.1016/j.nanoen.2014.12.019

Liu, J., Song, K., van Aken, P. A., Maier, J., and Yu, Y. (2014). Self-Supported $Li_4Ti_5O_{12}$-C Nanotube Arrays as High-Rate and Long-Life Anode Materials for Flexible Li-Ion Batteries. *Nano Lett.* 14 (5), 2597–2603. doi:10.1021/nl5004174

Liu, J., Tang, S., Lu, Y., Cai, G., Liang, S., Wang, W., et al. (2013). Synthesis of Mo_2N Nanolayer Coated MoO_2 Hollow Nanostructures as High-Performance Anode Materials for Lithium-Ion Batteries. *Energy Environ. Sci.* 6 (9), 2691–2697. doi:10.1039/c3ee41006d

Lu, Y., Zhang, Q., and Chen, J. (2019). Recent Progress on Lithium-Ion Batteries with High Electrochemical Performance. *Sci. China Chem.* 62 (5), 533–548. doi:10.1007/s11426-018-9410-0

Ma, Y., Ding, B., Ji, G., and Lee, J. Y. (2013). Carbon-Encapsulated F-Doped $Li_4Ti_5O_{12}$ as a High Rate Anode Material for Li+ Batteries. *ACS Nano* 7 (12), 10870–10878. doi:10.1021/nn404311x

Qu, X. L., Pu, K. C., Gao, M. X., Liu, Y. F., and Pan, H. G. (2018). Nanostructuring and Alloying of Si-Based Anode Materials. *Materials China* 037 (004), 254–263.

Shen, L., Zhang, X., Uchaker, E., Yuan, C., and Cao, G. (2012). $Li_4Ti_5O_{12}$ Nanoparticles Embedded in a Mesoporous Carbon Matrix as a Superior Anode Material for High Rate Lithium Ion Batteries. *Adv. Energy Mat.* 2 (6), 691–698. doi:10.1002/aenm.201100720

Shi, Y., Wen, L., Li, F., and Cheng, H.-M. (2011). Nanosized $Li_4Ti_5O_{12}$/graphene Hybrid Materials with Low Polarization for High Rate Lithium Ion Batteries. *J. Power Sources* 196 (20), 8610–8617. doi:10.1016/j.jpowsour.2011.06.002

Sun, X., Hegde, M., Wang, J., Zhang, Y., Liao, J., Radovanovic, P. V., et al. (2014). Structural Analysis and Electrochemical Studies of Carbon Coated $Li_4Ti_5O_{12}$ Particles Used as Anode for Lithium-Ion Battery. *ECS Trans.* 58 (14), 79–88. doi:10.1149/05814.0079ecst

Tan, Y., and Xue, B. (2018). Research Progress of Lithium Titanate as Anode Material for Lithium Ion Battery. *J. Inorg. Mater.* 33 (05), 475–482. doi:10.15541/jim20170330

Tang, Y., Yang, L., Qiu, Z., and Huang, J. (2009). Template-free Synthesis of Mesoporous Spinel Lithium Titanate Microspheres and Their Application in High-Rate Lithium Ion Batteries. *J. Mat. Chem.* 19 (33), 5980–5984. doi:10.1039/b907480e

Wang, D. D. (2020). Studies of Ti-Based Oxide Anode Materials for Lithium Ion Battery. Doctoral Dissertation. Tianjin: Tianjin University.

Wang, J., Zhao, H., Yang, Q., Wang, C., Lv, P., and Xia, Q. (2013). $Li_4Ti_5O_{12}$-TiO_2 Composite Anode Material for Lithium-Ion Batteries. *J. Power Sources* 222, 196–201. doi:10.1016/j.jpowsour.2012.08.082

Wang, Q., Geng, J., Yuan, C., Kuai, L., and Geng, B. (2016). Mesoporous Spherical $Li_4Ti_5O_{12}$/TiO_2 Composites as an Excellent Anode Material for Lithium-Ion Batteries. *Electrochimica Acta* 212, 41–46. doi:10.1016/j.electacta.2016.06.153

Wang, Y. J. (2021). Preparation and Electrochemical Properties of Titanate Anode Materials for Lithium Ion Batteries. MS Dissertation. Wulumuqi: Xinjiang Normal University.

Xu, Z., Yin, Q., Li, X., Meng, Q., Xu, L., Lv, B., et al. (2020). Self-assembly of a Highly Stable and Active Co_3O_4/H-TiO_2 Bulk Heterojunction with High-Energy Interfacial Structures for Low Temperature CO Catalytic Oxidation. *Catal. Sci. Technol.* 10 (24), 8374–8382. doi:10.1039/d0cy01477j

Yan, J. D. (2014). Development Status and Prospect Analysis of Lithium-Ion Battery. *J. Aeronautics* 35 (10), 2767–2775.

Yang, L. Y., Li, H. Z., Liu, J., Sun, Z. Q., Tang, S. S., and Lei, M. (2015). Dual Yolk-Shell Structure of Carbon and Silica-Coated Silicon for High-Performance Lithium-Ion Batteries. *Sci. Rep.* 5 (1), 10908–10909. doi:10.1038/srep10908

Yang, L. Y., Li, H. Z., Liu, J., Tang, S. S., Lu, Y. K., Li, S. T., et al. (2015). $Li_4Ti_5O_{12}$ Nanosheets as High-Rate and Long-Life Anode Materials for Sodium-Ion Batteries. *J. Mat. Chem. A* 3 (48), 24446–24452. doi:10.1039/c5ta07403g

Yang, X., Xu, C., Li, S., Wu, Y. P., Wu, X. Q., Yin, Y. M., et al. (2022). Thermal Treatment for Promoting Interfacial Interaction in Co-BDC/$Ti_3C_2T_X$ Hybrid Nanosheets for Hybrid Supercapacitors. *J. Colloid Interface Sci.* 617, 633–640. doi:10.1016/j.jcis.2022.03.015

You, S. L., Fang, L., Xu, H. T., and Wang, Y. (2018). Progress in the Research on Anode Material $Li_4Ti_5O_{12}$ for Li-Ion Batteries. *J. Chongqing Univ.* 41 (12), 92–100. doi:10.1183/j.issn.1000-582X.2018.12.011

Zettsu, N., Mizuno, Y., Kojima, H., Yubuta, K., Sakaguchi, T., Saito, T., et al. (2014). Direct Fabrication of Densely Packed Idiomorphic $Li_4Ti_5O_{12}$ Crystal Layers on Substrates by Using a LiCl-NaCl Mixed Flux and Their Additive-free Electrode Characteristics. *Cryst. Growth & Des.* 14 (11), 5634–5639. doi:10.1021/cg5009279

Zhang, C., Zhang, Y., Wang, J., Wang, D., He, D., and Xia, Y. (2013). $Li_4Ti_5O_{12}$ Prepared by a Modified Citric Acid Sol-Gel Method for Lithium-Ion Battery. *J. Power Sources* 236, 118–125. doi:10.1016/j.jpowsour.2013.01.135

Zhang, J., Wang, S., and Xu, G. (2021). Assembly of Multifunctional $Li_4Ti_5O_{12}$@Co_3O_4 Heterostructures for High-Performance Li-Ion Half/full Batteries[J]. *J. Alloys Compd.* 856, 158110. doi:10.1016/j.jallcom.2020.158110

Zhou, G. W., Lee, D. K., Kim, Y. H., Kim, C. W., and Kang, Y. S. (2006). Preparation and Spectroscopic Characterization of Ilmenite-Type $CoTiO_3$ Nanoparticles. *Bull. Korean Chem. Soc.* 27 (3), 368–372.

Conflict of Interest: The authors declare that the research was conducted in the absence of any commercial or financial relationships that could be construed as a potential conflict of interest.

Publisher's Note: All claims expressed in this article are solely those of the authors and do not necessarily represent those of their affiliated organizations or those of the publisher, the editors, and the reviewers. Any product that may be evaluated in this article, or claim that may be made by its manufacturer, is not guaranteed or endorsed by the publisher.